Article

Mechanistic Insights into the Binding of Boar Salivary Pheromones and Putative Molecule with Receptor Proteins: A Comparative Computational Approach

Devaraj Sankarganesh,*,# Ambritha Balasundaram,# George Priya Doss C,* Raghunath Azhwar, Shanmugam Achiraman, and Govindaraju Archunan
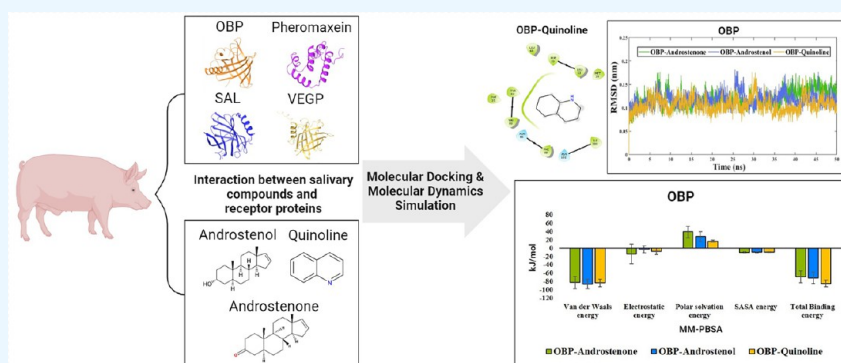
Read Online

| ACCESS | | Metrics & More | | Article Recommendations | | SI Supporting Information |

ABSTRACT: Precise estrus detection in sows is pivotal in increasing the productivity within the pork industry. Sows in estrus exhibit exclusive behaviors when exposed to either a live boar or the steroid pheromones androstenone and androstenol. Recently, a study employing solid-phase microextraction-gas chromatography−mass spectrometry has identified a novel salivary molecule in boars, known as quinoline. This finding has intriguing implications as a synthetic mixture of androstenone, androstenol, and quinoline induces estrus behaviors in sows. Nevertheless, the precise pheromonal characteristics of quinoline remain elusive. In this study, we validate and compare the binding efficiency of androstenone, androstenol, and quinoline with porcine olfactory receptor proteins (odorant-binding protein [OBP], pheromaxein, salivary lipocalin [SAL], and Von Ebner's gland protein [VEGP]) using molecular docking and molecular dynamics simulations. All protein−ligand complexes demonstrated stability, as evidenced by the root-mean-square deviation (RMSD), root-mean-square fluctuation (RMSF), radius of gyration (R_g), solvent-accessible surface area (SASA), and hydrogen-bond (H-bond) plots. Furthermore, quinoline displayed higher binding efficiency with OBP, measured at −85.456 ± 8.268 kJ/mol, compared to androstenone and androstenol, as determined by molecular mechanics—Poisson−Boltzmann surface area (MM-PBSA) calculations. Conversely, quinoline exhibited a lower binding efficacy when interacting with SAL, pheromaxein, and VEGP compared to androstenone and androstenol. These findings, in part, suggest the binding possibility of quinoline with carrier proteins and warrant further investigation to support the role of quinoline in porcine chemical communication.

INTRODUCTION

Pheromones are an important chemical signal class, regulating social behavior and reproduction across numerous vertebrate species. These chemical signals originate from various sources, including urine, feces, saliva, glandular secretions, cervical mucus, and so on.[1] Pheromones constitute a diverse array of volatile and semivolatile organic compounds, as well as nonvolatile proteins. The detection of these pheromonal cues is facilitated by a complex network of olfactory systems and subsystems, which include the main olfactory system, the vomeronasal organ (VNO), Grueneberg ganglion, and septal organ,[2] depending on the species. The intricate chemistry and sophisticated organization of these detection systems in

vertebrates underscore the ongoing need for a comprehensive understanding of this fascinating field.[3]

Pigs hold a prominent role in the livestock industry, and their reproduction significantly depends on pheromones. The detection of estrus, a critical event determining reproductive success in pigs, hinges on a combination of specific behavioral

displays and physical indicators exhibited by sows in the presence of a live boar.[4] In part, these behavioral responses of sows are elicited by pheromones secreted into boar saliva. Notably, the boars' submandibular gland is a major source of steroid pheromones.[5] A few androstene steroids identified within boar saliva and salivary gland extracts have been tested for their ability to induce estrus behaviors in sows.[6] Among them, two steroid pheromones, androstenone, and androstenol, provoked high incidence of estrus behaviors.[7] However, these steroid pheromones still do not fully replicate the effect of a live boar in stimulating estrus behaviors in sows. McGlone *et al.* demonstrated that quinoline (a novel molecule in boar saliva), combined with steroid pheromones, elicited high sexual behavioral scores in sows.[8] Specifically, quinoline substantially increased the incidence of pricked ears in sows. The molecule mixture (the combination of steroid pheromones and quinoline) improved the estrus detection rate and the sow reproductive performance.[8,9] These findings profoundly impact the pork industry, as they contribute to enhanced reproductive efficiency.

The olfactory system possesses many receptor proteins that selectively bind to chemical molecules. Of note, odorant-binding proteins (OBPs) in many vertebrates facilitate the binding and release of odors and semiochemicals.[10] Muthukumar *et al.* attested OBP in the nasal mucus of buffalo and highlighted their role in the binding of pheromones.[11] Both boars and sows also have OBPs, salivary lipocalin (SAL), and von Ebner's gland protein (VEGP) in their nasal mucosa and VNO.[12] Pheromaxein identified in the submandibular glands of boars binds to the steroid molecules.[13,14] SAL was identified as a unique protein with sequence similarity and functional diversity comparable to that of rodent lipocalins. Marchese *et al.* reported that SAL can bind to general odorants while specifically retaining androstenone as the bound ligand.[15] The binding cavity of SAL contains two polar residues within its active site along with several other hydrophobic residues, implying the potential for strong hydrogen bonding (H-bonding) and other polar interactions, as well as the presence of a cavity to bind with larger molecules.[16] Research has unveiled a correlation between the synthesis of pheromaxein and the functional maturities of testes. Furthermore, the concentration of pheromaxein in the submandibular gland is closely linked to the levels of steroids.[17] These receptor proteins, distributed within the olfactory systems, facilitate the binding of odorants and pheromones found in various secretions, contributing to the orchestration of olfactory signaling.

Considering the latest research on boar saliva, it is imperative to accumulate compelling evidence to support the notion of quinoline as a pheromone and further elucidate its role in chemical signaling. However, the role of quinoline in porcine chemical signaling remains relatively unexplored and warrants further investigation.[18] Several factors contribute to the necessity for additional research in this area, as outlined below:

1. Quinoline's limited presence: Quinoline was identified in the saliva of only three boars from a single farm, which raises the questions about its prevalence and significance across different populations of boars.[19]

2. Variability among boars: The absence of quinoline in boars from different farms[19] suggests potential variability in its production and secretion among different groups of boars.

3. Unexplored implications: The olfactory and neuro-endocrinological implications of quinoline in porcine

communication have not been thoroughly investigated, leaving a significant gap in our understanding of its role in chemical signaling.[18]

Given these considerations, a comprehensive evaluation of the interaction of quinoline with receptor proteins in the olfactory system becomes crucial. Therefore, we intend to examine and compare the interactions of quinoline and steroid pheromones with four different binding/carrier proteins: pheromaxein, SAL, OBP, and VEGP. Computational approaches are crucial for studying molecular interactions, offering insights into binding affinities and dynamic behaviors. Techniques like molecular docking and molecular dynamics simulations (MDS) allow detailed exploration of molecular–level interactions, enhancing our understanding of complex mechanisms.[20−22] Therefore, we perform an *in silico* analysis of quinoline and steroid pheromones involving molecular docking, molecular dynamics, and molecular mechanics-Poisson–Boltzmann surface area calculations. This comparative analysis holds the potential to provide valuable insights into the pheromonal properties of quinoline and contribute to our understanding of its role in porcine chemical signaling. By investigating the molecular interactions between quinoline and these key receptor proteins, we aim to shed light on the mechanisms underlying quinoline's effects on porcine behavior and reproduction.

■ METHODS

Proteins. The three-dimensional (3-D), crystalline structures of OBP (PDB ID:1DZK, resolution of 1.48 Å),[23] and SAL (PDB ID:1GM6, resolution of 2.13 Å),[24] were retrieved from the Research Collaboratory for Structural Bioinformatics—Protein Data Bank (RCSB-PDB).[25,26] Water molecules and heteroatoms were removed from the proteins, and any missing residues were constructed using PyMOL.[27] The 3-D crystal structure of pheromaxein and VEGP are currently unavailable; thus, we obtained AF-Q863D3-F1 and AF-P53715-F1 from the AlphaFold Protein Structure Database.[28] Subsequently, all protein structures underwent energy-minimization using the GROMOS96 program in the Swiss-PDB viewer.[29]

Compounds (Ligands) Acquisition and Preparation. The 3-D chemical structures of the steroidal ligands (androstenone and androstenol) and quinoline were obtained from the PubChem database, and polar hydrogen atoms were added to these structures.[30] Energy minimization was performed using the Merck Molecular Force Field (MMFF94) within the Avogadro software.[31]

Identification of Active Site Residues of the Olfactory Receptor Proteins. The active sites of the proteins were determined using the Computed Atlas of Surface Topography of Proteins (CASTp) server 3.0.[32] The key residues identified within the predicted binding pockets of these proteins are listed in the Supporting Information Table 1.

Molecular Docking. Following the incorporating Kollman charges, computing Gasteiger charges, and assigning AD4 type atoms for each protein, we saved them individually in PDBQT format using AutoDockTools (ADT) 4.2 (MGL tools 1.5.6).[33] In ADT, for each ligand, we navigated to "TorsionTree," used "Detect Root" to find the torsion tree center axis, set torsional degrees under "TorsionTree" after selecting "Ligand," and saved ligand coordinates in PDBQT format.[33] Autogrid established the grid box for protein active site residues with customized dimensions for the anticipated ligand-binding site. Molecular

docking analysis employed the Lamarckian genetic algorithm, performed nine times with varied conformation levels in triplicate using AutoDock Vina.[34] The automated process concluded after 250 000 energy evaluations. The resulting binding sites were computed, and the affinity between the ligand and protein was measured in kcal/mol. The methodology allowed us to assess different complexes at distinct positions, generating nine different conformations for each compound, based on their binding affinities. The selection of the best-docked conformation was based on several criteria, including binding affinity, low root-mean-square deviation (RMSD) value (<1 Å), and hydrogen bond (H-bond) interactions between the ligand and the protein within the complex. The protein−ligand complex structures were generated using PyMOL and two-dimensional (2-D) ligand interactions and visualized using Maestro−Schrödinger Suite.[35]

Molecular Dynamics Simulation. The binding modes and stabilities of the protein−ligand complexes listed in Table 1 were

Table 1. List of Protein−Ligand Complexes Used in the Docking and Dynamics Approaches

s. no	complex
1	OBP−androstenone
2	OBP−androstenol
3	OBP−quinoline
4	pheromaxein−androstenone
5	pheromaxein−androstenol
6	pheromaxein−quinoline
7	SAL−androstenone
8	SAL−androstenol
9	SAL−quinoline
10	VEGP−androstenone
11	VEGP−androstenol
12	VEGP−quinoline

investigated in a dynamic environment using the GROMACS version 2018.2[36] and CHARMM27 force field over a simulation period of 50 ns.[37] The receptor topology for the investigated proteins was generated by the pdb2gmx module using CHARMM27 force fields.[37] Ligand topologies for the investigated compounds were generated using the SwissParam servers.[38] Each protein−ligand complex was then solvated within a cubic box of the transferable intermolecular potential with a three-point (TIP3P) water model, leaving a margin of 10 Å between the protein and each side of the 3D box. To maintain charge neutrality, Na$^+$ and Cl$^−$ ions were added by using GROMACS tools. A maximum of 50 000 steps of the steepest descent minimization technique were applied to minimize the energy in the simulation system.[39] The solvent and ions were equilibrated in two restrained phases. The reference temperature for the *NVT* (isothermal-isochoric) ensemble was 300 K, and for the following *NPT* (isothermal−isobaric) ensemble, the reference pressure was 1.0 bar.

Finally, MDS was conducted on the equilibrium systems without controls. The leapfrog integrator was employed with a time step of 2 femtosecond (fs). LINCS served as the constraint algorithm for both *NVT* and *NPT* ensembles, as well as the production MD runs.[40] A short-range van der Waals threshold of 1.2 nm was applied. Temperature and pressure coupling were achieved by using a modified Berendsen thermostat and a Parrinello−Rahman barostat. The simulated trajectories were analyzed by using the GROMACS analysis tool. The programs

gmx rms, gmx rmsf, gmx gyrate, gmx sasa, and gmx hbond were used to determine the RMSD, root-mean-square fluctuation (RMSF), radius of gyration (R_g), solvent-accessible surface area (SASA), and H-bonds (intermolecular and intramolecular). Additionally, principal component analysis (PCA) was performed using gmx covar and gmx anaeig. Gmx sham and gmx xpm2 ps were employed to calculate the Gibbs free energy. These comprehensive analyses allowed for a detailed examination of the behavior and stability of the protein−ligand complexes during MDS.

Estimation of Binding Free Energy. The molecular mechanics-Poisson−Boltzmann surface area (MM-PBSA) calculations were conducted using the g_mmpbsa package in GROMACS to determine the free binding energy of the proteins with the ligands.[41] The bonded and nonbonded interactions of the protein−ligand complexes in a vacuum were estimated for the binding affinity during the last 25 ns of the MD trajectories. The binding energy was computed as the sum of the van der Waals, electrostatic, polar solvation, and SASA energies. These calculations provide valuable insights into the binding affinity of the protein−ligand complexes and help assess the strength and nature of their interactions.

■ RESULTS

Molecular Docking. Molecular docking was performed with androstenone, androstenol, and quinoline to the binding site of OBP, pheromaxein, SAL, and VEGP using Auto Dock Vina to explore the binding affinity. Following successful docking runs, we identified the best-docked conformations for each ligand against the respective proteins based on the criteria of the lowest binding affinity (RMSD <1 Å) and the number of H-bonds formed. The binding affinities and specific amino acid residues involved in interactions for the 12 complexes are listed in Table 2. We observed significant variations in binding among the ligands and different proteins, with distinct amino acid

Table 2. Docking Scores of the Complexes and the Interacting Residues (Amino Acids) in the Binding Pocket of the Protein

| complexes	docking score (kcal mol^{-1})	interacting residues
OBP−androstenone	−5.8	Phe10, Leu12, Val90, Ser91, Tyr92, Ala93
OBP−androstenol	−5.8	Asn148, Tyr20, Ile146, Leu129, Lys133
OBP-quinoline	−6.8	Leu68, Phe55, Leu53, Met39, Phe35, Tyr82, Val80, Asn86, Phe88, Asn102, Ile100
pheromaxein−androstenone	−7.3	Leu77, Lys59, Val62, Phe31, Phe34, Leu35
pheromaxein-androstenol	−6.9	Leu77, Leu81, Ile69, Ala66, Val62, Phe31, Phe34, Leu35
pheromaxein−quinoline	−5.1	Leu27, Ala26, Glu30, Lys59, Leu46, Phe49
SAL−androstenone	−6.5	Leu42, Ile167, Asp169, Lys164, Val154, Asp151, Lys150, Pro147
SAL-androstenol	−6.3	Glu37, Gly36, Ala35, Lys33, Arg141, Ser117, Tyr116
SAL−quinoline	−4.5	Phe177, Cys176, Arg175, Asp174, Ile173
VEGP−androstenone	−7.7	Val25, Gly26, Gln27, Leu29, Lys89, Gln92, Pro93, Phe94, Phe96
VEGP-androstenol	−7.3	Val25, Gly26, Gln27, Leu29, Lys89, Thr90, Gln92, Pro93, Phe94, Phe96
VEGP−quinoline	−5.3	Gln27, Leu29, Lys89, Thr90, Gln92, Pro93, Phe94, Phe96
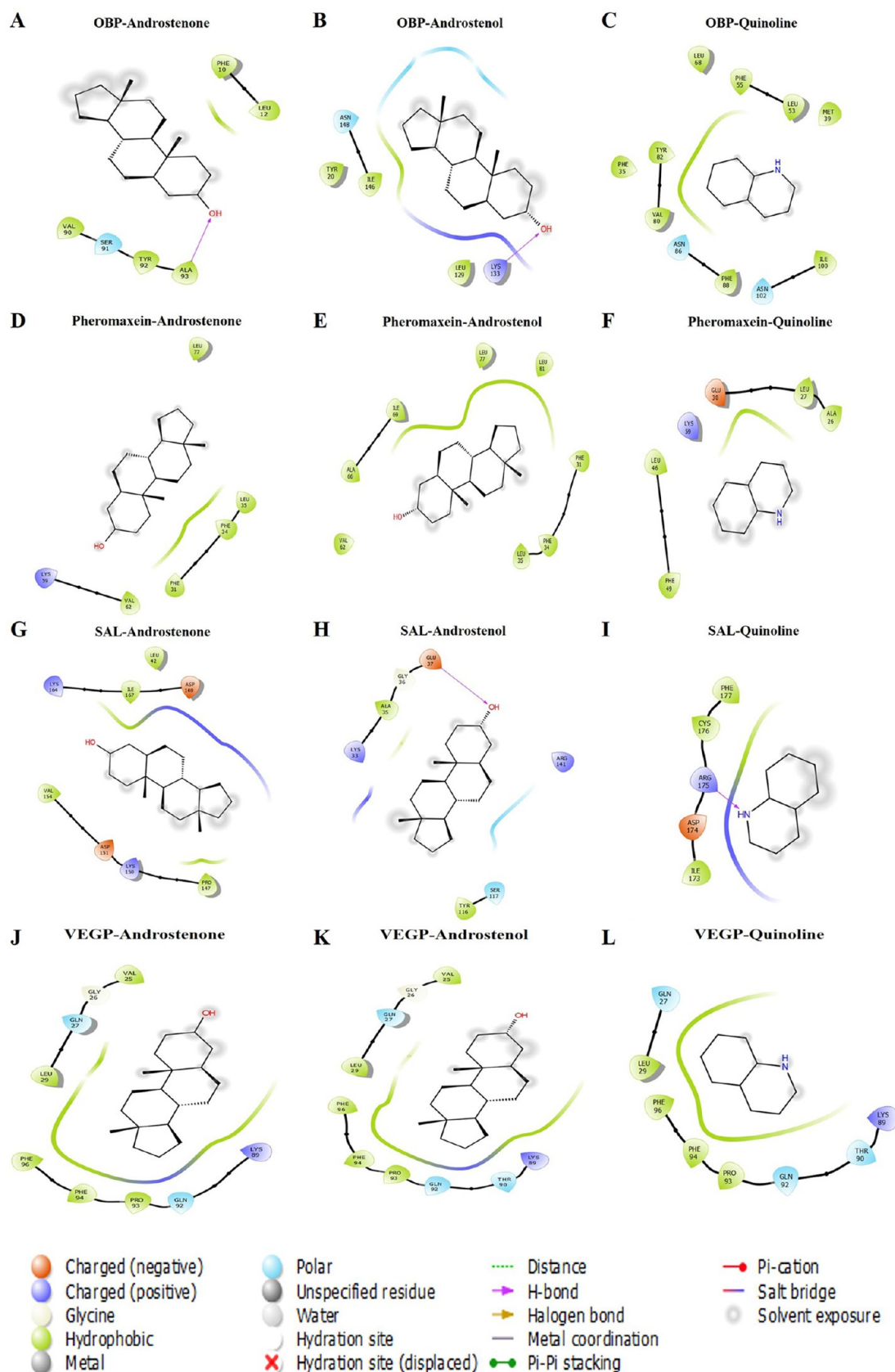
Figure 1. Two-dimensional representation of molecular interaction among the receptor protein−ligand complexes: (A) OBP−androstenone, (B) OBP−androstenol, (C) OBP−quinoline, (D) pheromaxein−androstenone, (E) pheromaxein−androstenol, (F) pheromaxein−quinoline, (G) SAL−androstenone, (H) SAL−androstenol, (I) SAL−quinoline, (J) VEGP−androstenone, (K) VEGP−androstenol, and (L) VEGP−quinoline.

residues participating in ligand interactions. When androstenone was docked with OBP, a binding affinity of -5.8 kcal mol^{-1} was achieved, and a single H-bond was formed with Ala93.

Interestingly, androstenol exhibited a similar binding affinity (-5.8 kcal mol^{-1}) when docked with OBP, but an H-bond was formed with the Lys133 residue. In contrast, quinoline displayed a lower binding affinity of -6.8 kcal mol^{-1} when docked with the OBP, without H-bond interactions. Pheromaxein docking with androstenone, androstenol, and quinoline yielded binding affinities of -7.3 kcal mol^{-1}, -6.9 kcal mol^{-1}, and -5.1 kcal mol^{-1}, respectively. Quinoline did not form an H-bond with pheromaxein. Docking of SAL with androstenone generated a binding affinity of -6.5 kcal mol^{-1} without H-bond interactions. Conversely, androstenol formed a H-bond with the Glu37 residue of SAL but with less binding affinity (-6.3 kcal mol^{-1}). Interestingly, quinoline formed an H-bond with the Arg175 residue of SAL, but the binding energy was the highest among all complexes in this study at -4.5 kcal mol^{-1}. Lastly, when docking with VEGP, androstenone and androstenol exhibited a binding affinity of -7.7 kcal mol^{-1} and -7.3 kcal mol^{-1} without H-bond interactions. In contrast, quinoline displayed a lower binding affinity of -5.3 kcal mol^{-1} without H-bond interactions. The docking experiments were conducted in triplicate, and the resulting docked complexes were visualized by using the Maestro-Schrödinger Suite. The 2-D representations of each complex were generated using the Maestro-Schrödinger Suite (Figure 1).

Molecular Dynamics Simulations. We conducted MDS to assess the internal dynamics, conformational alterations, and overall stability of both steroidal and putative quinoline ligands when interacting with various receptor proteins at an atomistic level. The MDS-generated trajectories for 12 protein−ligand complexes were subsequently analyzed for the following: RMSD, RMSF, R_g, SASA, and H-bonds (intramolecular and intermolecular). When binding at the active sites of the protein, the ligands may have produced conformational changes in their structures, and their respective average values are given in Table 3.

Root-Mean-Square Deviation. We conducted RMSD analyses for all simulated systems, focusing on the active sites of each protein when the ligands were bound. For OBP, the average RMSD values are ~0.12, ~0.12, and ~0.11 nm when bound with androstenone, androstenol, and quinoline,

respectively, indicating the stability of the protein structure in the presence of these ligands (Figure 2A). In pheromaxein, the average RMSD values of androstenone, androstenol, and quinoline are ~0.29, ~0.23, and ~0.29 nm, respectively (Figure 2B). Analyzing SAL, the average RMSD values are ~0.15, ~0.15, and ~0.10 nm when interacting with androstenone, androstenol, and quinoline, respectively (Figure 2C). VEGP's average RMSD values are ~0.18, ~0.16, and ~0.16 nm with androstenone, androstenol, and quinoline, respectively (Figure 2D). Overall, the RMSD values range from ~0.10 to ~0.29 nm, with the OBP, SAL, and VEGP complexes demonstrating relatively greater stability than the pheromaxein-ligand complexes, as indicated by their lower RMSD values.

Root-Mean-Square Fluctuation. RMSF graphs for the simulated complexes are depicted in Figure 3. RMSF values of the complexes of OBP−androstenone, OBP−androstenol, and OBP−quinoline were ~0.08, ~0.07, and ~0.07 nm, respectively. Androstenone and androstenol increased the flexibility of the beta-strands (residues 30−40, 58−62, and 108−115) (Figure 3A). RMSF value of pheromaxein−androstenol was ~0.16 nm higher than that of pheromaxein−androstenone and pheromaxein−quinoline complexes (~0.12 and ~0.13 nm) (Figure 3B). By contrast, RMSF value for SAL−androstenone (~0.09 nm) was higher compared to SAL−androstenol and SAL−quinoline (~0.08 and ~0.08 nm) (Figure 3C). Interestingly, the RMSF value for VEGP−androstenone (~0.11 nm) was moderately increased than that of other complexes (VEGP−androstenol and VEGP−quinoline), (which were ~0.09 and ~0.09 nm, respectively) (Figure 3D).

R_g. The overall R_g values were between 1.37 and 1.55 nm for all the proteins, with moderate variation in individual proteins. The R_g values for OBP−androstenone, OBP−androstenol, and OBP−quinoline complexes were similar (~1.48 nm) (Figure 4A), thus representing no significant alterations. The R_g values for the pheromaxein−androstenone, pheromaxein−androstenol, and pheromaxein−quinoline complexes were ~1.45, ~1.37, and ~1.39 nm, respectively (Figure 4B). The low R_g value of androstenol with pheromaxein indicates the high compactness of the complex. Similar to those of the OBP−ligand complexes, the average R_g values for the SAL−androstenone, SAL−androstenol, and SAL−quinoline complexes remain unchanged (~1.49 nm for all the complexes) (Figure 4C). Nevertheless, R_g values for VEGP with ligands showed a moderate variation (~1.55, ~1.53, and ~1.52 nm for VEGP-androstenone, VEGP−androstenol, and VEGP−quinoline, respectively) (Figure 4D).

Solvent Accessible Surface Area. The average SASA values of the OBP−androstenone, OBP−androstenol, and OBP−quinoline complexes were ~85.59, ~85.96, and ~84.64 nm^2, respectively (Figure 5A), thus affirming no significant structural differences upon binding of OBP with the ligands. However, the SASA for the OBP−quinoline complex was lower than that for other complexes. The average SASA values of the pheromaxein−androstenone, pheromaxein−androstenol, and pheromaxein−quinoline complexes were ~63.70, ~62.81, and ~64.16 nm^2, respectively (Figure 5B), wherein pheromaxein−androstenol showed lower values compared to other complexes. SASA values of SAL−androstenone (~85.49 nm^2) and SAL−quinoline (~85.23 nm^2) complexes were comparatively lower than those of SAL−androstenol (~87.15 nm^2) (Figure 5C). Conversely, SASA values for VEGP−ligand complexes were the highest. SASA values were ~96.13, ~94.14, and ~93.11 nm^2, respectively, for VEGP−androstenone, VEGP−androstenol, and VEGP−quinoline complexes (Figure 5D).

Table 3. Analysis of MDS Trajectories and the Respective Average Values of RMSD, RMSF, R_g, and SASA

| complexes	RMSD (nm)	RMSF (nm)	R_g (nm)	SASA (nm^2)
OBP−androstenone	~0.12	~0.08	~1.48	~85.59
OBP−androstenol	~0.12	~0.07	~1.48	~85.96
OBP−quinoline	~0.11	~0.07	~1.48	~84.64
pheromaxein−androstenone	~0.29	~0.12	~1.45	~63.70
pheromaxein−androstenol	~0.23	~0.16	~1.37	~62.81
pheromaxein−quinoline	~0.29	~0.13	~1.39	~64.16
SAL-androstenone	~0.15	~0.09	~1.49	~85.49
SAL-androstenol	~0.15	~0.08	~1.49	~87.15
SAL-quinoline	~0.10	~0.08	~1.49	~85.23
VEGP−androstenone	~0.18	~0.11	~1.55	~96.13
VEGP−androstenol	~0.16	~0.09	~1.53	~94.14
VEGP−quinoline	~0.16	~0.09	~1.52	~93.11
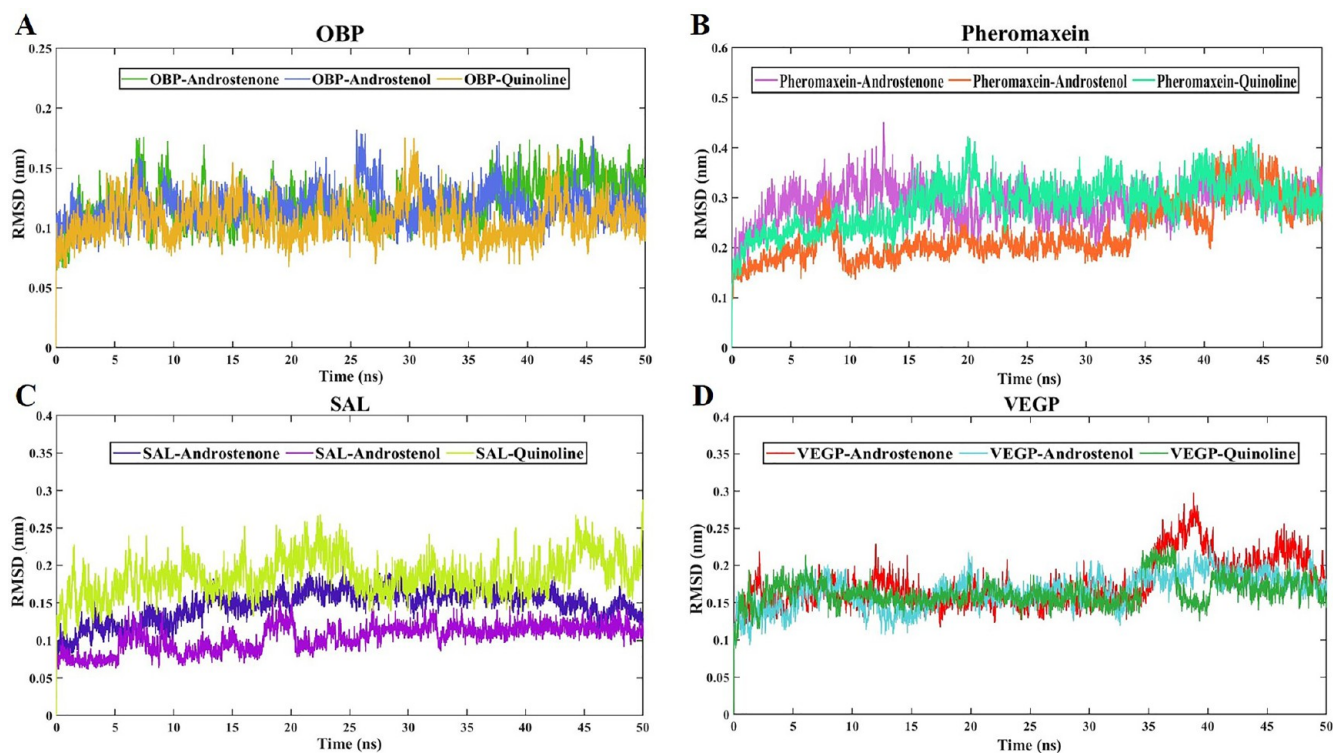
Figure 2. RMSD of the receptor protein−ligand complexes. On the RMSD in nanoseconds, while the *y*-axis illustrates the RMSD in nanometers. (A) OBP-androstenone (grass green color), OBP-androstenol (azure color), and OBP-Quinoline (mustard color); (B) pheromaxein-androstenone (lilac color), pheromaxein-androstenol (clay color), and pheromaxein-quinoline (sea foam color); (C) SAL-androstenone (navy blue color), SAL-androstenol (royal purple color), and SAL-quinoline (pear color); (D) VEGP-androstenone (red color), VEGP-androstenol (crystal blue color), and VEGP-quinoline (green color).
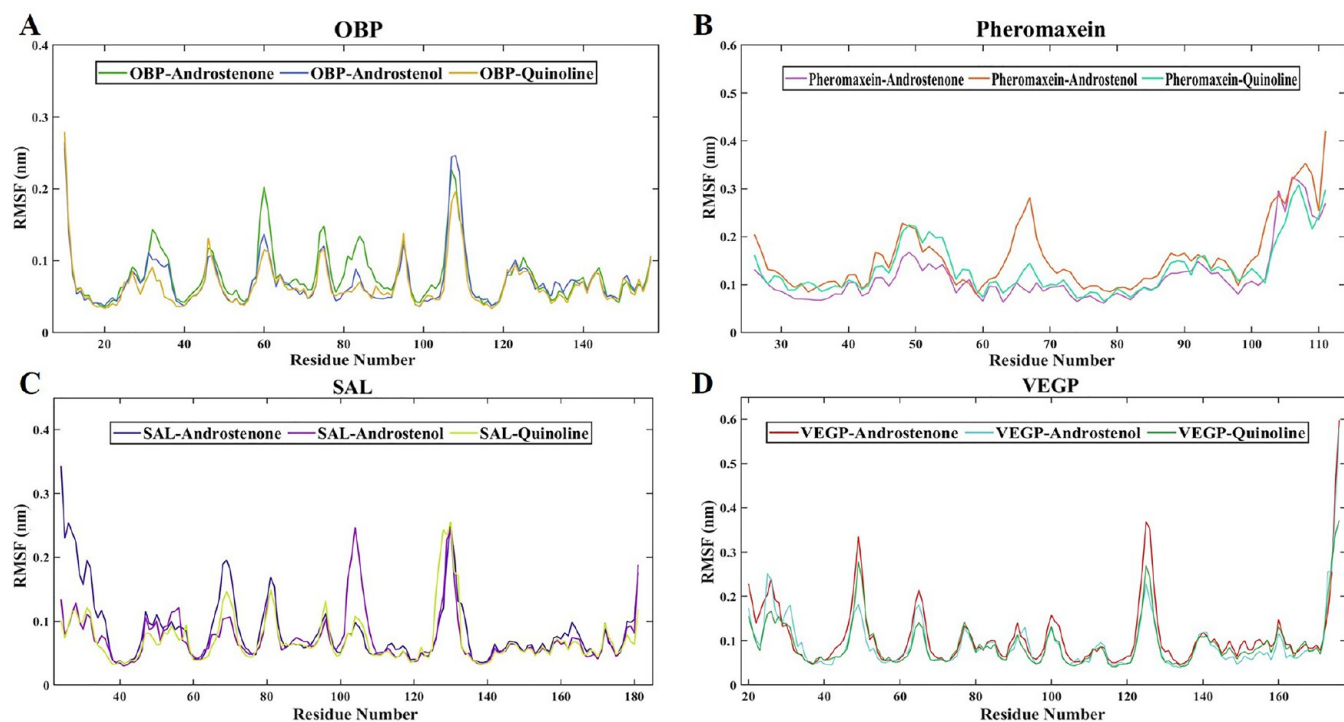

Figure 3. RMSF of receptor protein−ligand complexes. On the *x*-axis, the number of residues is depicted, while the *y*-axis illustrates the RMSF in nanometers. (A) OBP-androstenone (grass green color), OBP-androstenol (azure color), and OBP-quinoline (mustard color); (B) pheromaxein−androstenone (lilac color), pheromaxein−androstenol (clay color), and pheromaxein−quinoline (sea foam color); (C) SAL−androstenone (navy blue color), SAL−androstenol (royal purple color), and SAL-quinoline (pear color); (D) VEGP−androstenone (red color), VEGP−androstenol (crystal blue color), and VEGP−quinoline (green color).
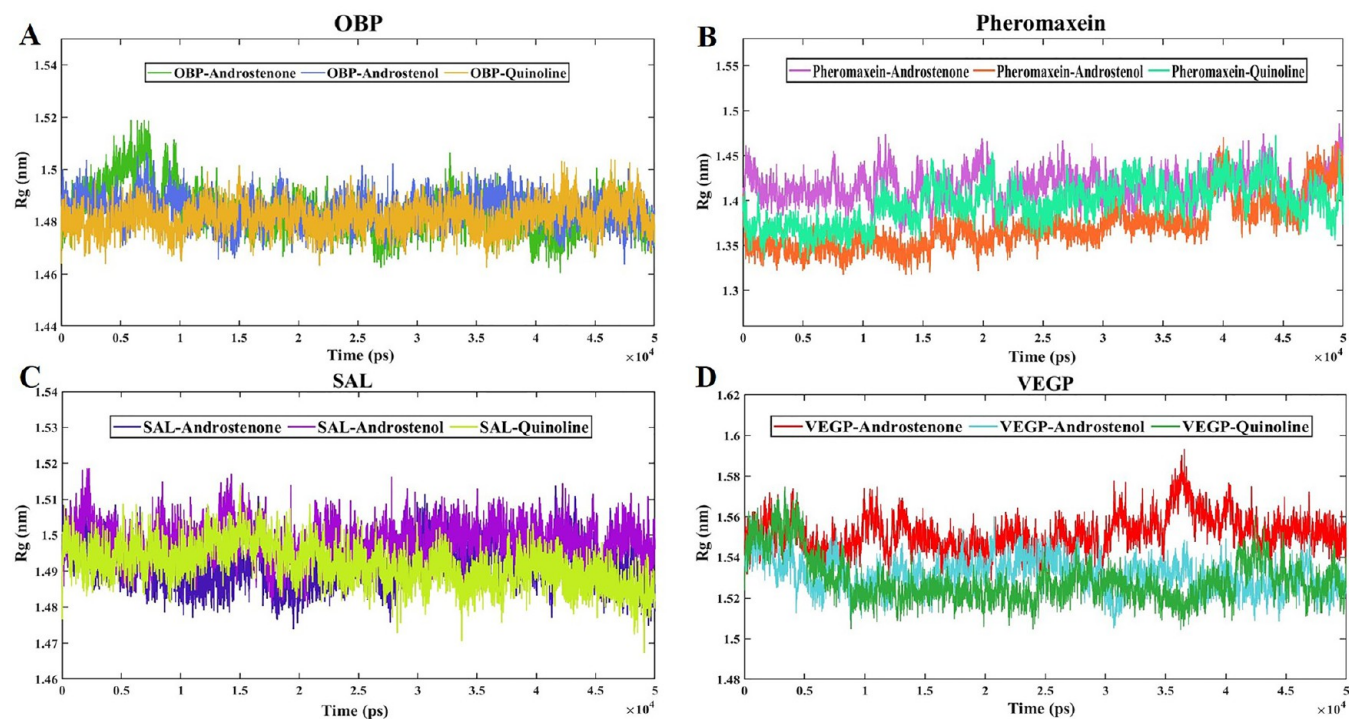
Figure 4. R_g of receptor protein−ligand complexes. On the x-axis, the time in picoseconds (ps), while the y-axis illustrates the R_g in nanometers. (A) OBP−androstenone (grass green color), OBP−androstenol (azure color), and OBP−quinoline (mustard color); (B) pheromaxein−androstenone (lilac color), pheromaxein−androstenol (clay color), and pheromaxein-quinoline (sea foam color); (C) SAL−androstenone (navy blue color), SAL−androstenol (royal purple color), and SAL−quinoline (pear color); (D) VEGP-androstenone (red color), VEGP−androstenol (crystal blue color), and VEGP−quinoline (green color).
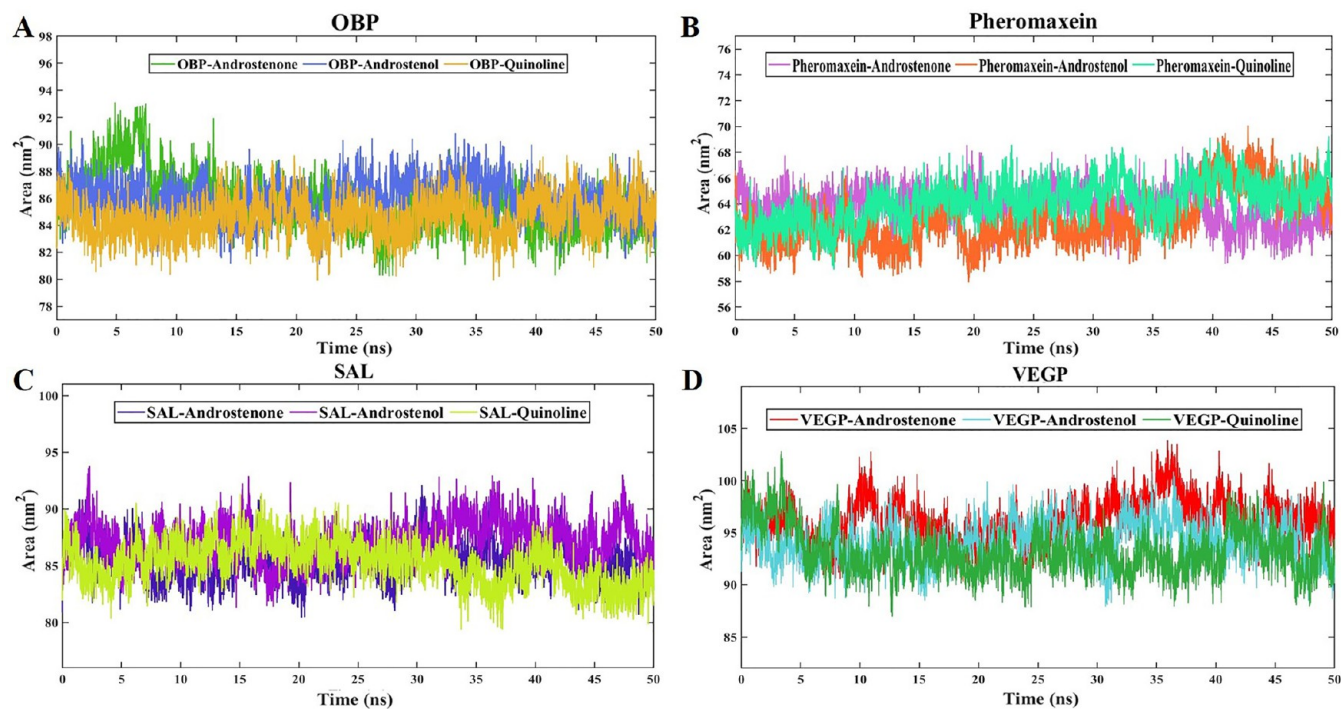
Figure 5. SASA of receptor protein−ligand complexes. On the x-axis, the time in nanoseconds (ns) is depicted, while the y-axis illustrates the area in square nanometers (nm^2). (A) OBP−androstenone (grass green color), OBP-androstenol (azure color), and OBP-quinoline (mustard color); (B) pheromaxein−androstenone (lilac color), pheromaxein−androstenol (clay color), and pheromaxein−quinoline (sea foam color); (C) SAL−androstenone (navy blue color), SAL−androstenol (royal purple color), and SAL−quinoline (pear color); (D) VEGP−androstenone (red color), VEGP−androstenol (crystal blue color), and VEGP−quinoline (green color).

Intramolecular and Intermolecular H-Bonding. The intramolecular H-bonds formed in the 12 complexes were calculated over 50 ns (Table 4; Figure 6). We found 114

Table 4. Number of Intramolecular and Intermolecular H-Bonds Formed in the Complexes

complexes	number of intramolecular H-bonds	number of intermolecular H-bonds
OBP−androstenone	~114	0−2
OBP−androstenol	~114	0−2
OBP−quinoline	~117	0−1
pheromaxein−androstenone	~62	0−1
pheromaxein-androstenol	~57	0−2
pheromaxein−quinoline	~60	0−1
SAL−androstenone	~117	0−1
SAL−androstenol	~117	0−2
SAL−quinoline	~125	0−1
VEGP−androstenone	~107	0−2
VEGP−androstenol	~107	0−2
VEGP−quinoline	~107	0−2

intramolecular H-bonds for OBP−androstenone and OBP−androstenol, which are similar but less than those of OBP−quinoline (Figure 6A). Of note, the least number of intramolecular H-bonds was found in pheromaxein−androstenone (62), pheromaxein−androstenol (57), and pheromaxein−quinoline (60) (Figure 6B). The number of intramolecular H-

bonds found in SAL−androstenone, SAL−androstenol, and SAL-quinoline was 117, 117, and 125, respectively (Figure 6C). VEGP−androstenone, VEGP−androstenol, and VEGP−quinoline were found to have an average of 107 intramolecular H-bonds (Figure 6D).

Next, we calculated the intermolecular H-bonds in the complexes (Table 4; Figure 7). OBP−androstenone, OBP−androstenol, and OBP−quinoline complexes had 0−2, 0−2, and 0−1 H-bonds, respectively (Figure 7A). The number of H-bonds was 0−1, 0−2, and 0−1 H-bonds in pheromaxein−androstenone, pheromaxein−androstenol, and pheromaxein−quinoline complexes, respectively (Figure 7B). Interestingly, the number of H-bonds for SAL-ligand complexes was the same as pheromaxein−ligand complexes in that SAL−androstenone, SAL−androstenol, and SAL−quinoline complexes had 0−1, 0−2, and 0−1 H-bonds, respectively (Figure 7C). The VEGP−androstenone, VEGP−androstenol, and VEGP−quinoline complexes had an invariable number of H-bonds (0−2 for all of the complexes) (Figure 7D).

PCA and Gibbs Free Energy. We found the OBP−quinoline complex to be more stable and exhibit lower correlated motions than those of the OBP−androstenone and OBP−androstenol (Figure 8A). Figure 8B shows that pheromaxein-androstenone occupied less correlated motions than the pheromaxein−androstenol and pheromaxein−quinoline complexes. Concurrently, the SAL−androstenone and SAL−androstenol complexes exhibited less correlated movements than SAL−quinoline (Figure 8C). Unlike other complexes, all VEGP−ligand complexes exhibited varied correlated motions (Figure 8D).
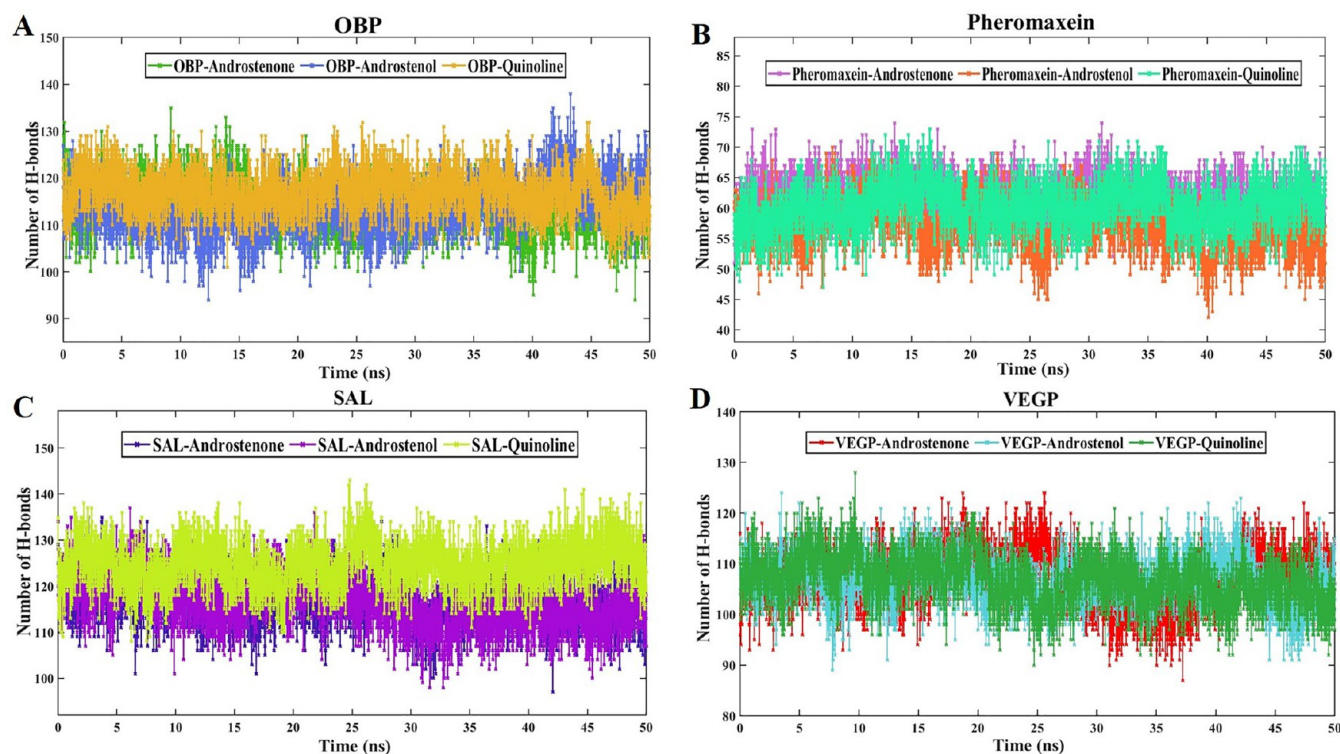

Figure 6. Intramolecular hydrogen bonds formed in the receptor proteins. On the *x*-axis, the time in nanoseconds (ns), while the *y*-axis illustrates the number of intramolecular H-bonds. (A) OBP−androstenone (grass green color), OBP−androstenol (azure color), and OBP−quinoline (mustard color); (B) pheromaxein−androstenone (lilac color), pheromaxein−androstenol (clay color), and pheromaxein−quinoline (sea foam color); (C) SAL−androstenone (navy blue color), SAL−androstenol (royal purple color), and SAL−quinoline (pear color); (D) VEGP-androstenone (red color), VEGP−androstenol (crystal blue color), and VEGP−quinoline (green color).
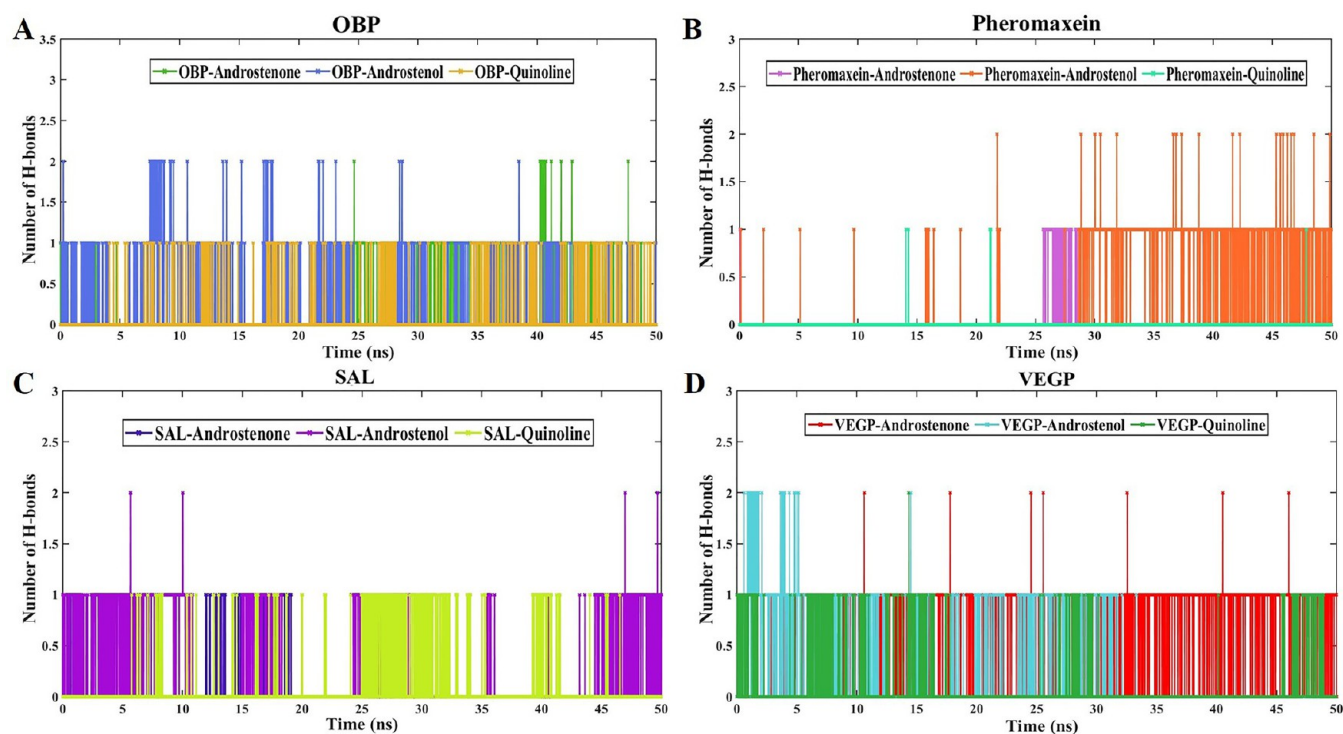
Figure 7. Intermolecular hydrogen bonds formed between the receptor protein–ligand complexes. On the *x*-axis, the time in nanoseconds (ns) is depicted, while the *y*-axis illustrates the number of intermolecular H-bonds. (A) OBP–androstenone (grass green color), OBP–androstenol (azure color), and OBP–quinoline (mustard color); (B) pheromaxein-androstenone (lilac color), pheromaxein-androstenol (clay color), and pheromaxein–quinoline (sea foam color); (C) SAL-androstenone (navy blue color), SAL–androstenol (royal purple color), and SAL–quinoline (pear color); (D) VEGP–androstenone (red color), VEGP–androstenol (crystal blue color), and VEGP–quinoline (green color).

The Gibbs free energy for principal components 1 and 2 of all 12 complexes is illustrated in Figure 9. The Gibbs free energies for the OBP–androstenone, OBP–androstenol, and the OBP–quinoline complexes were 0–10.5 kJ mol^{-1}, 0–10 kJ mol^{-1}, and 0–9.4 kJ mol^{-1}. The Gibbs free energies were 0–10.6 kJ mol^{-1}, 0–11.6 kJ mol^{-1}, and 0–10.5 kJ mol^{-1} for pheromaxein–androstenone, pheromaxein–androstenol, and pheromaxein–quinoline, respectively. SAL–androstenone, SAL–androstenol, and SAL–quinoline showed Gibbs free energy values of 0–10.8 kJ mol^{-1}, 0–10.9 kJ mol^{-1}, and 0–12 kJ mol^{-1}, respectively. The Gibbs free energies for VEGP–androstenone, VEGP–androstenol, and VEGP–quinoline complexes were 0–10.9 kJ mol^{-1}, 0–10.3 kJ mol^{-1}, and 0–12.2 kJ mol^{-1}, respectively. Many complexes (OBP–quinoline, pheromaxein–quinoline, SAL–androstenone, SAL–androstenol, and VEGP–androstenol) had an intense, blue-colored area in the heatmap, indicating a lower energy and thermodynamically stable complex.

MM-PBSA Calculation and Analysis of Binding Affinity. The sum of all the nonbonded interactions is the binding free energy, which was calculated using the MM-PBSA approach for all the complexes over the last 25 ns of MDS (Table 5). The binding free energies for the OBP–androstenone, OBP–androstenol, and OBP–quinoline complexes were −69.793 ± 14.564, −72.308 ± 13.875, and −85.456 ± 8.268 kJ mol^{-1}, respectively (Figure 10A). Pheromaxein–androstenone, pheromaxein–androstenol, and pheromaxein–quinoline complexes revealed binding free energies of −81.256 ± 11.373, −86.224 ± 28.933, and −10.836 ± 26.782 kJ mol^{-1}, respectively (Figure 10B). We found highly variable binding free energies for SAL–androstenone, SAL–androstenol, and SAL–quinoline complexes (−48.590 ± 15.181, −70.690 ± 18.377, and

−26.744 ± 21.500 kJ mol^{-1}, respectively) (Figure 10C). Remarkably, VEGP– androstenone and VEGP–androstenol complexes exhibited the highest binding energy than any other complexes of the present study (−133.622 ± 10.854 and −145.491 ± 35.151 kJ mol^{-1}) and was threefold higher than VEGP–quinoline complex (−30.188 ± 18.352 kJ mol^{-1}) (Figure 10D).

■ DISCUSSION

The chemical properties of the ligands play a critical role in determining their binding efficiency with proteins, which, in turn, initiates the neuroendocrine cascade during chemical signaling. *In silico* assessment of the likelihood of protein–ligand complex formation can be achieved through docking scores representing energy values. Our study evaluated the docking scores of three ligands in boar saliva (androstenone, androstenol, and quinoline) with four different proteins (OBP, pheromaxein, SAL, and VEGP). Our findings revealed that the steroidal ligands exhibited the best energy scores when binding with pheromaxein, SAL, and VEGP. Conversely, the OBP–quinoline complex displayed a lower energy value, indicating the possibility of effective binding. However, other quinoline complexes (pheromaxein–quinoline, SAL–quinoline, and VEGP–quinoline) showed higher energy values, suggesting that quinoline may be less effective in binding with pheromaxein, SAL, and VEGP compared to the steroidal ligands. In other studies, ligand-binding assays have revealed high-affinity interactions, such as the binding of oleic acid and p-cresol with buffalo nasal OBPs and lauric acid with Fel d1.[11,42] The docking score of p-cresol with β-lactoglobulin and OBP revealed the high-affinity binding of p-cresol with OBP.[43] It is not
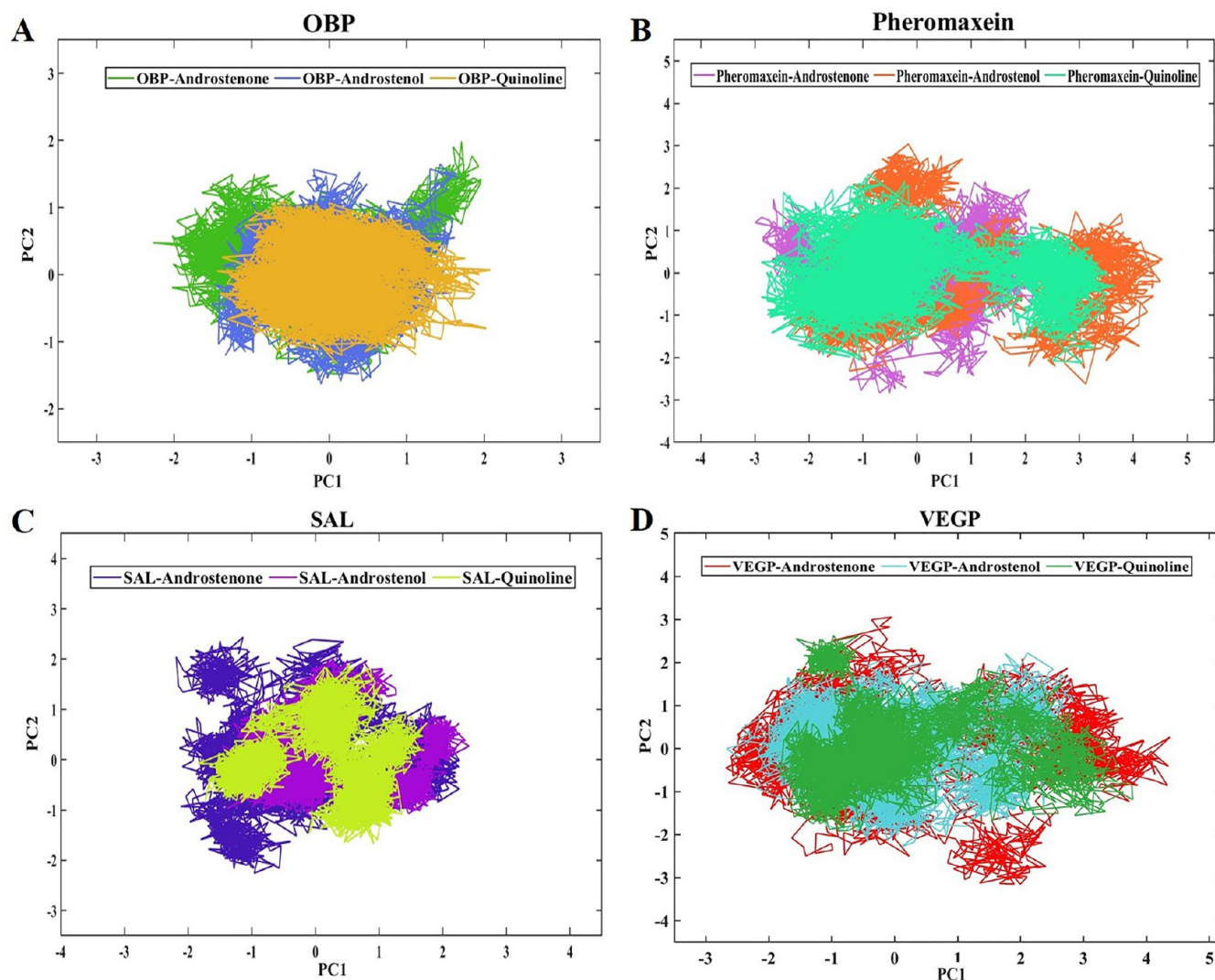
Figure 8. PCA of receptor protein−ligand complexes. On the *x*-axis, principal component 1 (PC1) is depicted, while the *y*-axis illustrates principal component 2 (PC2). (A) OBP−androstenone (grass green color), OBP−androstenol (azure color), and OBP−quinoline (mustard color); (B) pheromaxein−androstenone (lilac color), pheromaxein−androstenol (clay color), and pheromaxein−quinoline (sea foam color); (C) SAL−androstenone (navy blue color), SAL−androstenol (royal purple color), and SAL−quinoline (pear color); (D) VEGP−androstenone (red color), VEGP−androstenol (crystal blue color), and VEGP−quinoline (green color).

surprising that p-cresol is an estrus-specific pheromone identified in many body fluids.[44−46] Docking of mice pheromones (farnesol and 2-isobutyl-3-methoxypyranize) with estrus urinary lipocalin protein revealed high binding energy.[47] These studies underscore the importance of specific ligand−protein interactions in chemical communication. Moreover, the docking of mouse pheromones and the binding of (*z*)-7-dodecynyl acetate with African elephant trunk OBP further support the pheromonal nature of these compounds.[48] Our docking analysis suggests that steroidal ligands indeed exhibit pheromonal properties. However, quinoline could also be a partial component of the boar saliva, as evidenced by its low binding scores, albeit mainly with the OBP. Nevertheless, quinoline may have limited roles in inducing consummatory sexual behaviors in sows.

Next, we delved into the interactions between the ligands and proteins by examining the amino acid residues involved.[49] Quinoline exhibited interaction with 11 amino acid residues (Leu68, Phe55, Leu53, Met39, Phe35, Tyr82, Val80, Asn86, Phe88, Asn102, and Ile100) of the OBP, supporting our docking

results. It has been demonstrated that odorants of unrelated chemical structures can bind to pOBP with similar affinities by interacting with different amino acid residues in the binding pocket.[50] In contrast, SAL interacted with quinoline through only five residues (Phe177, Cys176, Arg175, Asp174, and Ile173), fewer than the steroid ligands. VEGP interacted with quinoline through eight residues with lower binding affinity (Gln27, Leu29, Lys89, Thr90, Gln92, Pro93, Phe94, and Phe96), compared to the steroid ligands. These findings imply that quinoline displays a strong interaction primarily with OBP but exhibits weaker interactions with other proteins compared to steroidal ligands. Hydrophobic amino acids appeared to play a significant role in these interactions, in line with previous studies highlighting the hydrophobic nature of odorants and binding pockets in carrier proteins.[51,52]

While docking analysis provided discernible information, assessing the conformational flexibility of protein−ligand complexes through MDS is equally important. In our study, we conducted an RMSD analysis to gauge the conformational flexibility of these complexes, which revealed interesting
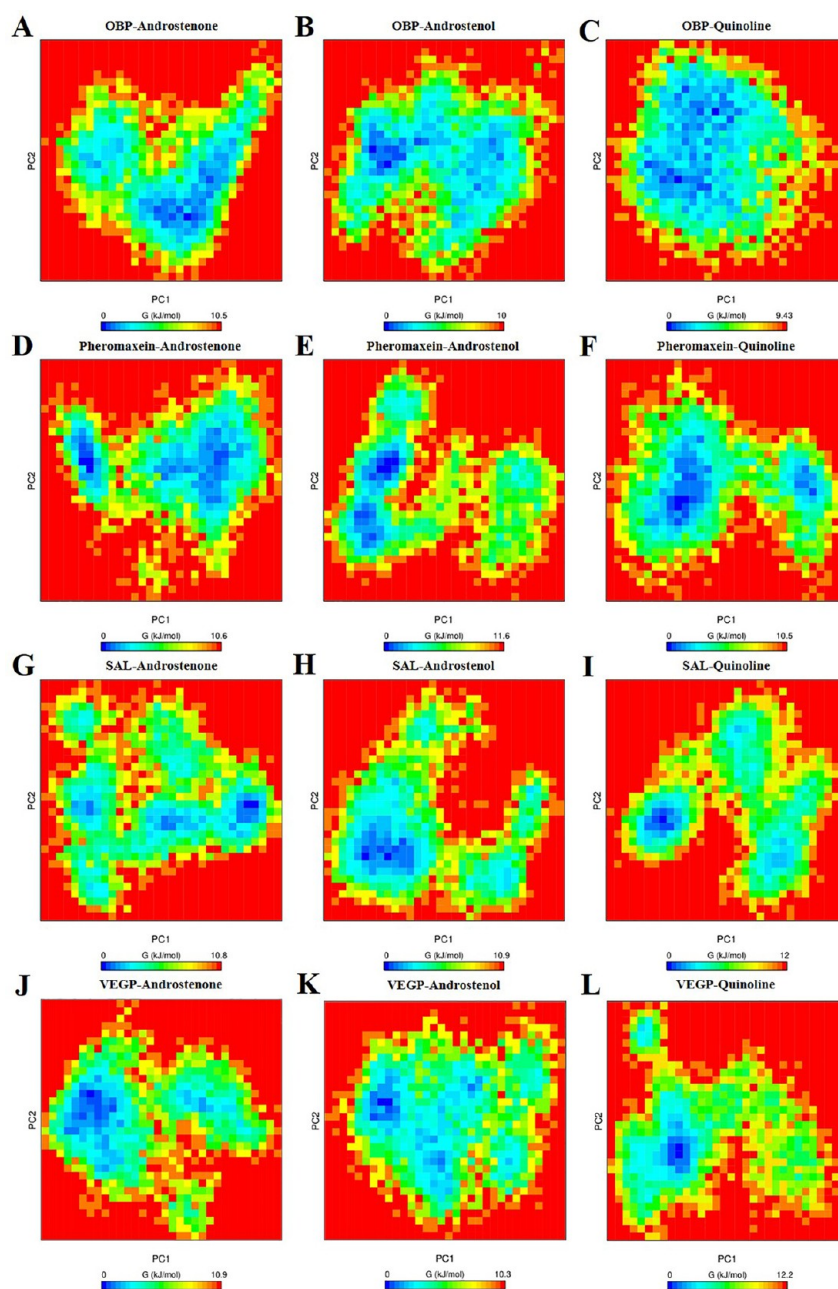
Figure 9. Gibbs free energy of various receptor protein—ligand complexes. The color bar indicates Gibbs free energies (in kJ/mol) corresponding to conformational states, ranging from minimum (blue) to maximum (red) energy levels. (A) OBP—androstenone, (B) OBP—androstenol, (C) OBP—quinoline, (D) pheromaxein—androstenone, (E) pheromaxein—androstenol, (F) pheromaxein—quinoline, (G) SAL—androstenone, (H) SAL—androstenol, (I) SAL—quinoline, (J) VEGP—androstenone, (K) VEGP—androstenol, and (L) VEGP—quinoline.

findings.[53] The RMSD of six ligands with buffalo nasal OBP (bunOBP) attained equilibrium at around three ns and remained relatively constant throughout the simulation, suggesting that bunOBP binds to the odors (ligands) and facilitates sexual communication in buffalo.[11] However, it is worth noting that we observed highly fluctuating RMSD values for some of the protein—ligand complexes during the simulation. Nonetheless, the complexes involving OBP, SAL, and VEGP appeared relatively stable, as evidenced by their RMSD values.

We also examined the RMSF, which implies the structural flexibility of the proteins, by analyzing fluctuations in protein residues.[54] Interestingly, the RMSF values of pheromaxein—ligands and VEGP—ligands were comparatively higher than those of the OBP—ligands and SAL—ligands complexes,

indicating the higher flexibility of pheromaxein and VEGP. In particular, pheromaxein-androstenol exhibited the highest RMSF value, suggesting pronounced flexibility. Furthermore, the RMSF of VEGP—androstenone was relatively higher than that of the VEGP—androstenol and VEGP—quinoline complexes, indicating the high flexibility of VEGP. Quinoline exhibited a higher RMSF and greater flexibility when interacting with pheromaxein compared to other proteins (OBP, SAL, and VEGP). OBP-p-cresol complex revealed a high fluctuation of 20 residues at both alpha termini of OBP, as judged by the high RMSF values, rendering support for OBP in contrast to our results.[55] Nevertheless, the RMSF of many protein—ligand complexes is highly correlated with RMSD. Zhao *et al.* suggest high RMSF as an indicator of increased flexibility of the residues

Table 5. Calculation of Binding Free Energy of the Complexes

| complexes	van der Waals energy (±SD) kJ mol^{-1}	electrostatic energy (±SD) kJ mol^{-1}	polar solvation energy (±SD) kJ mol^{-1}	SASA energy (±SD) kJ mol^{-1}	Total Binding energy (±SD) kJ mol^{-1}
OBP−androstenone	−83.359 ± 14.932	−14.459 ± 23.333	38.559 ± 14.322	−10.533 ± 1.297	−69.793 ± 14.564
OBP−androstenol	−86.731 ± 11.477	−3.026 ± 8.863	27.675 ± 11.689	−10.226 ± 1.259	−72.308 ± 13.875
OBP−quinoline	−84.120 ± 9.300	−7.872 ± 7.475	16.331 ± 2.562	−9.795 ± 0.769	−85.456 ± 8.268
pheromaxein−androstenone	−79.538 ± 9.294	−4.637 ± 18.444	13.725 ± 19.305	−10.806 ± 0.802	−81.256 ± 11.373
pheromaxein−androstenol	−98.669 ± 13.887	−15.034 ± 13.091	39.375 ± 18.667	−11.897 ± 1.151	−86.224 ± 28.933
pheromaxein−quinoline	−8.241 ± 13.448	−0.993 ± 3.088	−0.064 ± 24.604	−1.538 ± 2.059	−10.836 ± 26.782
SAL−androstenone	−86.634 ± 9.082	−1.941 ± 3.428	50.309 ± 18.026	−10.324 ± 0.677	−48.590 ± 15.181
SAL−androstenol	−89.087 ± 11.994	−4.214 ± 6.897	31.827 ± 16.298	−9.216 ± 1.257	−70.690 ± 18.377
SAL−quinoline	−28.658 ± 19.064	−9.403 ± 9.696	15.168 ± 19.284	−3.852 ± 2.593	−26.744 ± 21.500
VEGP−androstenone	−143.716 ± 11.246	−14.864 ± 5.660	40.529 ± 6.155	−15.571 ± 0.81	−133.622 ± 10.854
VEGP−androstenol	−150.073 ± 25.933	−2.782 ± 4.331	23.556 ± 10.759	−16.191 ± 1.297	−145.491 ± 35.151
VEGP−quinoline	−26.411 ± 21.163	−6.958 ± 8.358	7.297 ± 25.669	−4.115 ± 2.984	−30.188 ± 18.352
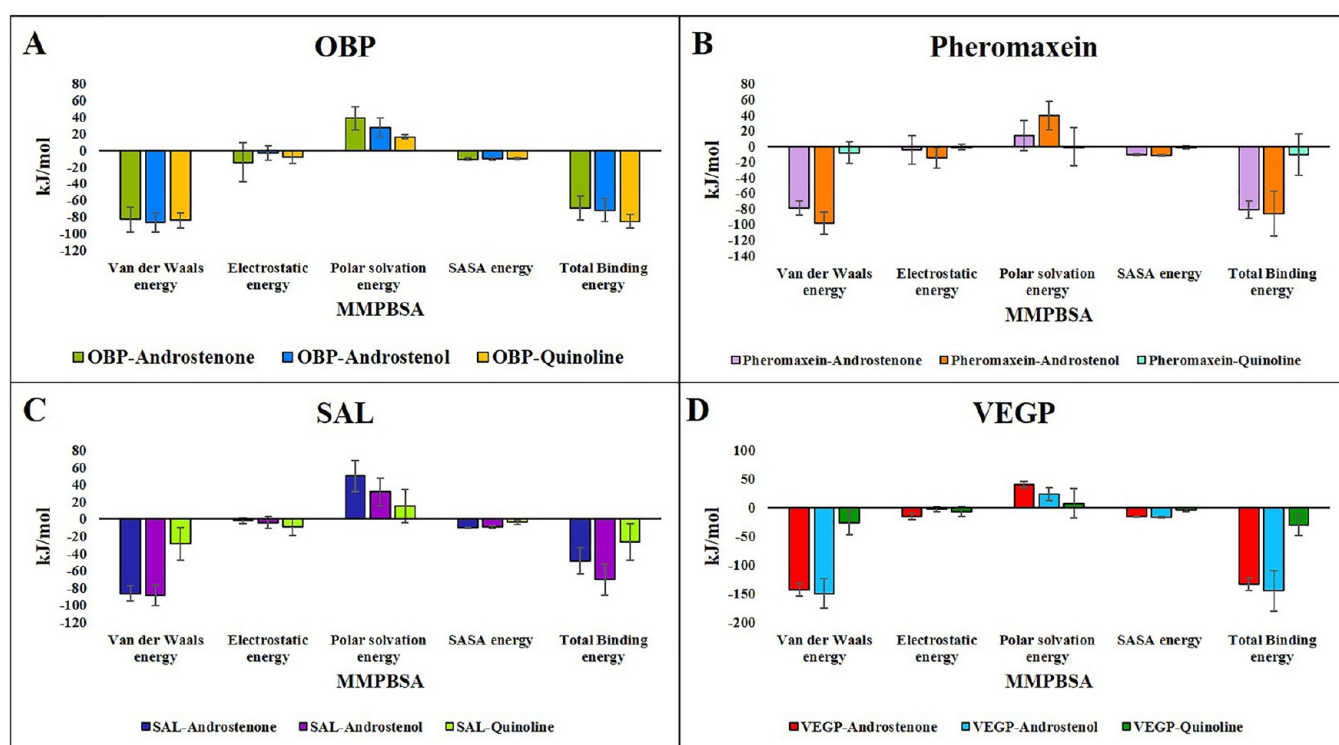
Figure 10. Binding free energy of the receptor protein−ligand complexes exhibited by various energy forms. (A) OBP−androstenone (grass green color), OBP−androstenol (azure color), and OBP−quinoline (mustard color); (B) pheromaxein−androstenone (lilac color), pheromaxein−androstenol (clay color), and pheromaxein−quinoline (sea foam color); (C) SAL−androstenone (navy blue color), SAL−androstenol (royal purple color), and SAL−quinoline (pear color); (D) VEGP−androstenone (red color), VEGP−androstenol (crystal blue color), and VEGP−quinoline (green color).

that bind with the ligands.[56] In agreement with this and based on RMSD and RMSF, we propose pheromaxein and VEGP as the most flexible proteins and androstenol and androstenone as the favorable ligands.

The compactness of the protein−ligand complexes was assessed through R_g values, which we found to be highly correlated to the RMSD values. Ligands exhibiting elevated R_g values tend to possess greater flexibility, rendering them more prone to instability. Conversely, lower R_g values signify conformations that are tightly packed and densely structured. This analysis aids in discerning the stability and flexibility of ligands within the molecular system under investigation.[57] The

R_g values remain constant for stable proteins but fluctuate for relatively unstable proteins, thus denoting the loss of compactness.[58,59] In our study, pheromaxein−ligand complexes exhibited the lowest R_g values, implying the high compactness of pheromaxein compared to that of other proteins. This suggests that pheromaxein is the most stable protein among the complexes. Although the R_g values differed for the other three protein−ligand complexes, they did not vary considerably. R_g values indicate that pheromaxein is the only stable protein. The VEGP-ligand complexes exhibited the highest R_g values, indicating low compactness, contrary to RMSF data but in concert with RMSD results. Given the R_g values, it is highly

plausible to attribute pheromaxein to a key protein in porcine chemical communication. Indeed, pheromaxein is found only in the submandibular gland of boars and is secreted into saliva along with steroids.[12] The high SASA values were inferred to contribute to the flexibility and extended conformation.[60] However, SASA analysis provided contrasting results with the lowest SASA values for pheromaxein–ligand complexes. In contrast, SASA values for other protein–ligand complexes were high, aligning with the RMSD data. These conflicting results from RMSD, RMSF, R_g, and SASA analyses suggest that the behavior of these complexes is complex and may be influenced by multiple factors.

H-bonds are involved in protein folding and stability, contributing to the intrinsic flexibility of proteins.[61] Intermolecular H-bonds and intramolecular H-bonds serve different functions, with intermolecular H-bonds improving the enthalpic term of the free energy of binding, while intramolecular H-bonds stabilize the interface between the molecule and proteins.[62] In our analysis, we observed a high number of intramolecular H-bonds in the SAL–ligand and the OBP–ligand complexes, with quinoline exhibiting the highest number of intramolecular H-bonds. Conversely, the fewest intramolecular H-bonds were observed in pheromaxein–ligands, whereas VEGP–ligands had a moderate number. Remarkably, SAL–quinoline and OBP–quinoline complexes exhibited a higher number of H-bonds compared with other protein-steroid complexes. This observation contrasts with a study by Durairaj et al., which reports increased H-bonds between Fel d1 and certain ligands (proven feline pheromones) but decreased H-bonds between Fel d1 and androstenone.[63] However, in our study, androstenone showed many H-bonds only with pheromaxein. The analysis of intramolecular H-bonds reveals two significant findings. First, it supports the established role of androstenone as a porcine pheromone. Second, it provides evidence that quinoline may indeed be a salivary molecule with potential pheromonal properties. We anticipate similar findings for the intermolecular H-bonds. However, it is worth noting that intermolecular H-bonds for quinoline appeared to be lower when interacting with three proteins (OBP, pheromaxein, and SAL).

Finally, we calculated the free binding energies of the protein–ligand complexes. The lowest free binding energy was attributed to effective binding, in that pyrido-fused imidazo[4,5-c]quinoline derivative binds effectively with phosphoinositide 3-kinase.[64] In our study, pheromaxein–quinoline, SAL–quinoline, and VEGP–quinoline complexes exhibited low free binding energies. However, the free energy of the OBP–quinoline was higher than those of the OBP–androstenone and OBP–androstenol. Given this notion and taking support from intramolecular H-bonds, we suggest quinoline as a putative molecule owing to its low binding free energy with the three receptor proteins.

Lastly, the compounds' solubility and size can influence their binding efficiency to receptor proteins. For instance, a study by Moitrier et al. showed that the pyrazine analogs exhibited low-level nonspecific binding with mouse OBP5, whereas odorants of different chemical classes showed increased binding affinity.[51] Our study consistently observed a strong binding affinity for the high molecular weight steroid ligands. In contrast, quinoline is a relatively low molecular weight heterocyclic compound, which may contribute to its distinct binding with receptor proteins.

Our study aligns with and further supports the findings of Guiraudie et al. and provides several key points to consider in the context of porcine chemical signaling:[65]

1. Guiraudie et al. proposed VEGP as a potential receptor for steroids, especially testosterone. Our data aligns with this proposal, as limited evidence supports VEGP's role as a receptor protein.[65]

2. SAL isoform identified in the VNO revealed a high binding affinity toward progesterone and oleic acid, suggesting structural similarities between progesterone and androstenone/androstenol. Our study partially supports this idea, as we found evidence of SAL's interaction with androstenone and androstenol.

3. Our study provides convincing evidence that pheromaxein binds to steroids and quinoline, reinforcing its significance in porcine chemical signaling.

4. It is conceivable that the perception and discrimination of different odor molecules (ligands studied here) in pigs could be achieved by synergistic or sequential activation of different proteins in both the nasal mucosa and the VNO. This concept has already been demonstrated in mice, where the main olfactory system and the VNO synergistically detect pheromones.[66]

Finally, the studies by Manikkaraja et al. on buffaloes and Zhu et al. on giant pandas highlight the diversity of OBPs and their differential affinities for various ligands.[55,67] These findings suggest that different isoforms of OBPs and potentially other receptor proteins may also exist in the Suidae family. These isoforms could serve as carriers for various ligands, enhancing the efficiency of chemical communication in pigs.

■ CONCLUSIONS

The study highlights quinoline's superior binding efficiency with OBP, supporting its potential role in the boar pheromone mixture based on MM-PBSA calculations. Overall, the results offer valuable insights into the molecular dynamics of pheromone binding, advancing our understanding of potential olfactory cues in boars. Though the mechanistic insights into the binding of various ligands with different receptor proteins are revealed in silico, the function of quinoline is still obscure. To establish quinoline as a pheromone, a more extensive sampling of boars from diverse populations is required to determine its frequency and variability, and thereby to understand the factors influencing quinoline production and its role in chemical communication. Research should delve deeper into how quinoline interacts with the porcine olfactory system and the resulting behavioral and physiological responses in sows. Our data offer partial support for the potential binding of quinoline with receptor proteins, shedding light on its involvement in chemical communication. Furthermore, we present empirical evidence of the significance of salivary molecules in boars, which play a crucial role in inducing estrus behaviors and hold commercial importance. However, it is important to note that this proof-of-principle study warrants further in vivo investigation to validate our findings. This research serves as a foundational step for future experimental studies, offering a platform for a deeper exploration of the broader spectrum of porcine pheromones and their functional roles. In summary, while the presence of quinoline in boar saliva is intriguing, further research is essential to determine its prevalence, variability, and precise role in porcine chemical signaling. Addressing these questions will contribute significantly to our understanding of this putative molecule (quinoline) and its potential impact on pigs' behavior and reproductive success. Eventually, a more comprehensive understanding of porcine

chemical signaling can affect various aspects of pig husbandry, reproduction, and the pork industry.

ASSOCIATED CONTENT

Supporting Information

The Supporting Information is available free of charge at https://pubs.acs.org/doi/10.1021/acsomega.3c09211.

(PDF)

AUTHOR INFORMATION

Corresponding Authors

George Priya Doss C − *School of Bio Sciences and Technology, Vellore Institute of Technology, Vellore 632014 Tamilnadu, India*; Email: georgepriyadoss@vit.ac.in

Devaraj Sankarganesh − *School of Bio Sciences and Technology, Vellore Institute of Technology, Vellore 632014 Tamilnadu, India*; orcid.org/0000-0001-7200-7816; Email: sankarganesh.d@vit.ac.in

Authors

Ambritha Balasundaram − *School of Bio Sciences and Technology, Vellore Institute of Technology, Vellore 632014 Tamilnadu, India*

Raghunath Azhwar − *Department of Pediatrics, University of Michigan School of Medicine, Ann Arbor, Michigan 48109, United States*

Shanmugam Achiraman − *Department of Environmental Biotechnology, Bharathidasan University, Tiruchirappalli 620024 Tamil Nadu, India*; orcid.org/0000-0002-6790-5205

Govindaraju Archunan − *School of Life Sciences, Marudupandiyar College, Thanjavur 613403 Tamil Nadu, India*

Complete contact information is available at:
https://pubs.acs.org/10.1021/acsomega.3c09211

Author Contributions

#D.S. and A.B. equal first authors. D.S., G.P.D.C., and R.A. were involved in the design of study, and A.B. performed the analyses. D.S., A.B., G.P.D.C., and R.A. drafted the manuscript. D.S., A.B., G.P.D.C., R.A., S.A., and G.A. improved the draft and revision of the manuscript. D.S. and G.P.D.C. supervised the entire study.

Notes

The authors declare no competing financial interest.

ACKNOWLEDGMENTS

REFERENCES

(1) Tirindelli, R.; Dibattista, M.; Pifferi, S.; Menini, A. From pheromones to behavior. *Physiol. Rev.* **2009**, *89* (3), 921−956.

(2) Liberles, S. D. Mammalian pheromones. *Annu. Rev. Physiol.* **2014**, *76*, 151−175.

(3) Brunjes, P. C.; Feldman, S.; Osterberg, S. K. The Pig Olfactory Brain: A Primer. *Chem. Senses* **2016**, *41* (5), 415−425.

(4) Kemp, B.; Soede, N. M.; Langendijk, P. Effects of boar contact and housing conditions on estrus expression in sows. *Theriogenology* **2005**, *63* (2), 643−656.

(5) Pearce, G. P.; Hughes, P. E.; Booth, W. D. The involvement of boar submaxillary salivary gland secretions in boar-induced precocious puberty attainment in the gilt. *Anim. Reprod. Sci.* **1988**, *16*, 125−134.

(6) Booth, W.; Diane Williamson, E.; Patterson, R. 16-androstene steroids in the submaxillary salivary gland of the boar in relation to measures of boar taint in carcasses. *Anim. Prod.* **1986**, *42* (1), 145−152.

(7) Melrose, D. R.; Reed, H. C.; Patterson, R. L. Androgen steroids associated with boar odour as an aid to the detection of oestrus in pig artificial insemination. *Br. Vet. J.* **1971**, *127* (10), 497−502.

(8) McGlone, J. J.; Devaraj, S.; Garcia, A. A novel boar pheromon.e mixture induces sow estrus behaviors and reproductive success. *Appl. Anim. Behav Sci.* **2019a**, *219*, 104832.

(9) McGlone, J. J.; Garcia, A.; Rakhshandeh, A. Multi-Farm Analyses Indicate a Novel Boar Pheromone Improves Sow Reproductive Performance. *Animals* **2019b**, *9* (2), 37.

(10) Pelosi, P.; Iovinella, I.; Felicioli, A.; Dani, F. R. Soluble proteins of chemical communication: an overview across arthropods. *Front. Physiol.* **2014**, *5*, 320.

(11) (a) Muthukumar, S.; Rajesh, D.; Selvam, R. M.; Saibaba, G.; Suvaithenamudhan, S.; Akbarsha, M. A.; Padmanabhan, P.; Gulyas, B.; Archunan, G. Buffalo nasal odorant-binding protein (bunOBP) and its structural evaluation with putative pheromones. *Sci. Rep.* **2018**, *8* (1), 9323. (b) Muthukumar, S.; Rajesh, D.; Selvam, R. M.; Saibaba, G.; Suvaithenamudhan, S.; Akbarsha, M. A.; Padmanabhan, P.; Gulyas, B.; Archunan, G. Author Correction: Buffalo nasal odorant-binding protein (bunOBP) and its structural evaluation with putative pheromones. *Sci. Rep.* **2018**, *8* (1), 11785.

(12) Sankarganesh, D.; Kirkwood, R. N.; Nagnan-Le Meillour, P.; Angayarkanni, J.; Achiraman, S.; Archunan, G. Pheromones, binding proteins, and olfactory systems in the pig (Sus scrofa): An updated review. *Front. Vet. Sci.* **2022**, *9*, 989409.

(13) Booth, W. D.; White, C. A. The isolation, purification and some properties of pheromaxein, the pheromonal steroid-binding protein, in porcine submaxillary glands and saliva. *J. Endocrinol.* **1988**, *118* (1), 47−57.

(14) Booth, W. D.; von Glos, K. I. Pheromaxein, the pheromonal steroid-binding protein, is a major protein synthesized in porcine submaxillary salivary glands. *J. Endocrinol.* **1991**, *128* (2), 205−212.

(15) Marchese, S.; Pes, D.; Scaloni, A.; Carbone, V.; Pelosi, P. Lipocalins of boar salivary glands binding odours and pheromones. *Eur. J. Biochem.* **1998**, *252* (3), 563−568.

(16) Sung, N.-D.; Park, C. S.; Park, H. Y.; Kim, C. K. Docking and virtual screening studies for new leads of boar salivary lipocalin. *Bull. Korean Chem. Soc.* **2008**, *29*, 959−962.

(17) Babol, J.; Squires, E. J.; Bonneau, M. Factors regulating the concentrations of 16-androstene steroids in submaxillary salivary glands of pigs. *J. Anim. Sci.* **1996**, *74* (2), 413−419.

(18) Sankarganesh, D.; Kirkwood, R.; Angayarkanni, J.; Achiraman, S.; Archunan, G. Pig pheromones and behaviors: A review. *Theriogenology* **2021**, *175*, 1−6.

(19) May, M. Use of solid-phase microextraction to detect semiochemicals in synthetic and biological samples. M. S. Thesis. Texas Tech University: TX; 2016.

(20) Sun, L.; Li, Y.; Zhang, Z.; Guo, H.; Xiao, Q.; Wang, Q.; Zhang, Y. Expression Patterns and Ligand Binding Characterization of Plus-C Odorant-Binding Protein 14 from Adelphocoris Lineolatus (Goeze). *Comp. Biochem. Physiol., Part B: Biochem. Mol. Biol.* **2019**, *227*, 75−82.

(21) Patel, R.; Singh, B.; Sharma, A.; Saraswat, J.; Dohare, N.; ud din Parray, M.; Siddiquee, M. A.; Alanazi, A. M.; Khan, A. A. Interaction and Esterase Activity of Albumin Serums with Orphenadrine: A Spectroscopic and Computational Approach. *J. Mol. Struct.* **2021**, *1239*, 130522.

(22) Kongot, M.; Maurya, N.; Dohare, N.; ud din Parray, M.; Maurya, J. K.; Kumar, A.; Patel, R. Enthalpy-Driven Interaction between Dihydropyrimidine Compound and Bovine Serum Albumin: A

Spectroscopic and Computational Approach. *J. Biomol. Struct. Dyn.* **2018**, *36* (5), 1161−1170.

(23) Vincent, F.; Spinelli, S.; Ramoni, R.; Grolli, S.; Pelosi, P.; Cambillau, C.; Tegoni, M. Complexes of porcine odorant binding protein with odorant molecules belonging to different chemical classes. *J. Mol. Biol.* **2000**, *300* (1), 127−139.

(24) Spinelli, S.; Vincent, F.; Pelosi, P.; Tegoni, M.; Cambillau, C. Boar salivary lipocalin: Three-dimensional X-ray structure and androstenol/androstenone docking simulations. *Eur. J. Biochem.* **2002**, *269* (10), 2449−2456.

(25) Kouranov, A.; Xie, L.; de la Cruz, J.; Chen, L.; Westbrook, J.; Bourne, P. E.; Berman, H. M. The RCSB PDB Information Portal for Structural Genomics. *Nucleic Acids Res.* **2006**, *34* (90001), D302−D305.

(26) Rose, P. W.; Bi, C.; Bluhm, W. F.; Christie, C. H.; Dimitropoulos, D.; Dutta, S.; Green, R. K.; Goodsell, D. S.; Prlic, A.; Quesada, M.; Quinn, G. B.; Ramos, A. G.; Westbrook, J. D.; Young, J.; Zardecki, C.; Berman, H. M.; Bourne, P. E. The RCSB Protein Data Bank: New Resources for Research and Education. *Nucleic Acids Res.* **2012**, *41* (D1), D475−D482.

(27) Lill, M. A.; Danielson, M. L. Computer-Aided Drug Design Platform Using PyMOL. *J. Comput. Aided Mol. Des.* **2011**, *25* (1), 13−19.

(28) Varadi, M.; Anyango, S.; Deshpande, M.; Nair, S.; Natassia, C.; Yordanova, G.; Yuan, D.; Stroe, O.; Wood, G.; Laydon, A.; Žídek, A.; Green, T.; Tunyasuvunakool, K.; Petersen, S.; Jumper, J.; Clancy, E.; Green, R.; Vora, A.; Lutfi, M.; Figurnov, M.; Cowie, A.; Hobbs, N.; Kohli, P.; Kleywegt, G.; Birney, E.; Hassabis, D.; Velankar, S. AlphaFold Protein Structure Database: Massively Expanding the Structural Coverage of Protein-Sequence Space with High-Accuracy Models. *Nucleic Acids Res.* **2022**, *50* (D1), D439−D444.

(29) Guex, N.; Peitsch, M. C. SWISS-MODEL and the Swiss-PdbViewer: An Environment for Comparative Protein Modeling. *Electrophoresis* **1997**, *18* (15), 2714−2723.

(30) Kim, S.; Thiessen, P. A.; Bolton, E. E.; Chen, J.; Fu, G.; Gindulyte, A.; Han, L.; He, J.; He, S.; Shoemaker, B. A.; Wang, J.; Yu, B.; Zhang, J.; Bryant, S. H. PubChem Substance and Compound Databases. *Nucleic Acids Res.* **2016**, *44* (D1), D1202−D1213.

(31) Hanwell, M. D.; Curtis, D. E.; Lonie, D. C.; Vandermeersch, T.; Zurek, E.; Hutchison, G. R. Avogadro: An Advanced Semantic Chemical Editor, Visualization, and Analysis Platform. *J. Cheminf.* **2012**, *4* (1), 17.

(32) Binkowski, T. A.; Naghibzadeh, S.; Liang, J. CASTp: Computed Atlas of Surface Topography of Proteins. *Nucleic Acids Res.* **2003**, *31* (13), 3352−3355.

(33) Morris, G. M.; Huey, R.; Lindstrom, W.; Sanner, M. F.; Belew, R. K.; Goodsell, D. S.; Olson, A. J. AutoDock4 and AutoDockTools4: Automated Docking with Selective Receptor Flexibility. *J. Comput. Chem.* **2009**, *30* (16), 2785−2791.

(34) Trott, O.; Olson, A. J. AutoDock Vina: Improving the Speed and Accuracy of Docking with a New Scoring Function, Efficient Optimization, and Multithreading. *J. Comput. Chem.* **2010**, *31* (2), 455−461.

(35) Lalitha, P.; Firdhouse, M. J. Maestro 9.4 as a Tool in the Structure Based Screening of Glycoalkaloids and Related Compounds, Targeting Aldose Reductase. *Trends Bioinf.* **2015**, *8* (1), 26−36.

(36) Abraham, M. J.; Murtola, T.; Schulz, R.; Páll, S.; Smith, J. C.; Hess, B.; Lindahl, E. GROMACS: High Performance Molecular Simulations through Multi-Level Parallelism from Laptops to Super-computers. *SoftwareX* **2015**, *1−2*, 19−25.

(37) Vanommeslaeghe, K.; Hatcher, E.; Acharya, C.; Kundu, S.; Zhong, S.; Shim, J.; Darian, E.; Guvench, O.; Lopes, P.; Vorobyov, I.; Mackerell, A. D. CHARMM General Force Field: A Force Field for Drug-like Molecules Compatible with the CHARMM All-Atom Additive Biological Force Fields. *J. Comput. Chem.* **2010**, *31* (4), 671−690.

(38) Zoete, V.; Cuendet, M. A.; Grosdidier, A.; Michielin, O. SwissParam: A Fast Force Field Generation Tool for Small Organic Molecules. *J. Comput. Chem.* **2011**, *32* (11), 2359−2368.

(39) Fliege, J.; Svaiter, B. F. Steepest Descent Methods for Multicriteria Optimization. *Math. Methods Oper. Res.* **2000**, *51* (3), 479−494.

(40) Hess, B.; Bekker, H.; Berendsen, H. J. C.; Fraaije, J. G. E. M. LINCS: A Linear Constraint Solver for Molecular Simulations. *J. Comput. Chem.* **1997**, *18* (12), 1463−1472.

(41) Kumari, R.; KumarLynn, R. A.; Lynn, A. G_mmpbsa−a GROMACS Tool for High-Throughput MM-PBSA Calculations. *J. Chem. Inf. Model.* **2014**, *54* (7), 1951−1962.

(42) Bienboire-Frosini, C.; Durairaj, R.; Pelosi, P.; Pageat, P. The Major Cat Allergen Fel d 1 Binds Steroid and Fatty Acid Semio-chemicals: A Combined In Silico and In Vitro Study. *Int. J. Mol. Sci.* **2020**, *21* (4), 1365.

(43) Karthikeyan, K.; Manivannan, P.; Rajesh, D.; Muthukumar, S.; Muralitharan, G.; Akbarsha, M. A.; Archunan, G. Identification of p-Cresol as an Estrus-Specific Volatile in Buffalo Saliva: Comparative Docking Analysis of Buffalo OBP and *β*-Lactoglobulin with p-Cresol. *Zool. Sci.* **2014**, *31* (1), 31−36.

(44) Rajanarayanan, S.; Archunan, G. Identification of urinary sex pheromones in female buffaloes and their influence on bull reproductive behaviour. *Res. Vet. Sci.* **2011**, *91* (2), 301−305.

(45) Muniasamy, S.; Muthu Selvam, R.; Rajanarayanan, S.; Ramesh Saravanakumar, V.; Archunan, G. p-cresol and oleic acid as reliable biomarkers of estrus: evidence from synchronized Murrah buffaloes. *Iran. J. Vet. Res.* **2017**, *18* (2), 124−127.

(46) Karthikeyan, K.; Muniasamy, S.; SankarGanesh, D.; Achiraman, S.; Ramesh Saravanakumar, V.; Archunan, G. Faecal chemical cues in water buffalo that facilitate estrus detection. *Anim. Reprod. Sci.* **2013**, *138* (3−4), 163−167.

(47) Rajesh, D.; Muthukumar, S.; Saibaba, G.; Siva, D.; Akbarsha, M. A.; Gulyás, B.; Padmanabhan, P.; Archunan, G. Structural elucidation of estrus urinary lipocalin protein (EULP) and evaluating binding affinity with pheromones using molecular docking and fluorescence study. *Sci. Rep.* **2016**, *6*, 35900.

(48) Zaremska, V.; Renzone, G.; Arena, S.; Ciaravolo, V.; Buberl, A.; Balfanz, F.; Scaloni, A.; Knoll, W.; Pelosi, P. An odorant-binding protein in the elephant's trunk is finely tuned to sex pheromone (Z)-7-dodecenyl acetate. *Sci. Rep.* **2022**, *12* (1), 19982.

(49) Senior, T.; Botha, M. J.; Kennedy, A. R.; Calvo-Castro, J. Understanding the Contribution of Individual Amino Acid Residues in the Binding of Psychoactive Substances to Monoamine Transporters. *ACS Omega* **2020**, *5* (28), 17223−17231.

(50) Vincent, F.; Spinelli, S.; Ramoni, R.; Grolli, S.; Pelosi, P.; Cambillau, C.; Tegoni, M. Complexes of porcine odorant binding protein with odorant molecules belonging to different chemical classes. *J. Mol. Biol.* **2000**, *300*, 127−139.

(51) Moitrier, L.; Belloir, C.; Lalis, M.; Hou, Y.; Topin, J.; Briand, L. Ligand Binding Properties of Odorant-Binding Protein OBP5 from Mus musculus. *Biology* **2022**, *12* (1), 2.

(52) Ilayaraja, R.; Rajkumar, R.; Rajesh, D.; Muralidharan, A. R.; Padmanabhan, P.; Archunan, G. Evaluating the binding efficiency of pheromone binding protein with its natural ligand using molecular docking and fluorescence analysis. *Sci. Rep.* **2014**, *4*, 5201.

(53) Northey, T.; Venthur, H.; De Biasio, F.; Chauviac, F. X.; Cole, A.; Ribeiro, K. A. L.; Grossi, G.; Falabella, P.; Field, L. M.; Keep, N. H.; Zhou, J. J. Crystal Structures and Binding Dynamics of Odorant-Binding Protein 3 from two aphid species Megoura viciae and Nasonovia ribisnigri. *Sci. Rep.* **2016**, *6*, 24739.

(54) Sharma, J.; Kumar Bhardwaj, V.; Singh, R.; Rajendran, V.; Purohit, R.; Kumar, S. An in-silico evaluation of different bioactive molecules of tea for their inhibition potency against non structural protein-15 of SARS-CoV-2. *Food Chem.* **2021**, *346*, 128933.

(55) Manikkaraja, C.; Bhavika, M.; Singh, R.; Nagarathnam, B.; George, G.; Gulyani, A.; Archunan, G.; Sowdhamini, R. Molecular and functional characterization of buffalo nasal epithelial odorant binding proteins and their structural insights by in silico and biochemical approaches. *J. Biomol. Struct. Dyn.* **2022**, *40* (9), 4164−4187.

(56) Zhao, Y.; Zeng, C.; Massiah, M. A. Molecular dynamics simulation reveals insights into the mechanism of unfolding by the

A130T/V mutations within the MID1 zinc-binding Bbox1 domain. *PLoS One* **2015**, *10* (4), No. e0124377.

(57) Baammi, S.; Daoud, R.; El Allali, A. In Silico Protein Engineering Shows That Novel Mutations Affecting NAD+ Binding Sites May Improve Phosphite Dehydrogenase Stability and Activity. *Sci. Rep.* **2023**, *13* (1), 1878.

(58) Chen, J.; Zaer, S.; Drori, P.; Zamel, J.; Joron, K.; Kalisman, N.; Lerner, E.; Dokholyan, N. V. The structural heterogeneity of *α*-synuclein is governed by several distinct subpopulations with interconversion times slower than milliseconds. *Structure* **2021**, *29* (9), 1048−1064.e6.

(59) Choudhary, S.; Kesavan, A. K.; Juneja, V.; Thakur, S. Molecular modeling, simulation and docking of Rv1250 protein from *Mycobacterium tuberculosis*. *Front. Bioinf.* **2023**, *3*, 1125479.

(60) Al-Subaie, A. M.; Kamaraj, B. The Structural Effect of FLT3Mutations at 835th Position and Their Interaction with Acute Myeloid Leukemia Inhibitors: In Silico Approach. *Int. J. Mol. Sci.* **2021**, *22* (14), 7602.

(61) Coimbra, J. T. S.; Feghali, R.; Ribeiro, R. P.; Ramos, M. J.; Fernandes, P. A. The importance of intramolecular hydrogen bonds on the translocation of the small drug piracetam through a lipid bilayer. *RSC Adv.* **2021**, *11* (2), 899−908.

(62) Erijman, A.; Rosenthal, E.; Shifman, J. M. How structure defines affinity in protein-protein interactions. *PLoS One* **2014**, *9* (10), No. e110085.

(63) Durairaj, R.; Pageat, P.; Bienboire-Frosini, C. Impact of Semiochemicals Binding to Fel d 1 on Its 3D Conformation and Predicted B-Cell Epitopes Using Computational Approaches. *Int. J. Mol. Sci.* **2023**, *24* (14), 11685.

(64) Dasmahapatra, U.; Kumar, C. K.; Das, S.; Subramanian, P. T.; Murali, P.; Isaac, A. E.; Ramanathan, K.; Mm, B.; Chanda, K. *In-silico* molecular modelling, MM/GBSA binding free energy and molecular dynamics simulation study of novel pyrido fused imidazo[4,5-*c*]quinolines as potential anti-tumor agents. *Front. Chem.* **2022**, *10*, 991369.

(65) Guiraudie, G.; Pageat, P.; Cain, A. H.; Madec, I.; Nagnan-Le Meillour, P. Functional characterization of olfactory binding proteins for appeasing compounds and molecular cloning in the vomeronasal organ of pre-pubertal pigs. *Chem. Senses* **2003**, *28* (7), 609−619.

(66) Achiraman, S.; Ponmanickam, P.; Ganesh, D. S.; Archunan, G. Detection of estrus by male mice: synergistic role of olfactory-vomeronasal system. *Neurosci. Lett.* **2010**, *477* (3), 144−148.

(67) Zhu, J.; Arena, S.; Spinelli, S.; Liu, D.; Zhang, G.; Wei, R.; Cambillau, C.; Scaloni, A.; Wang, G.; Pelosi, P. Reverse chemical ecology: Olfactory proteins from the giant panda and their interactions with putative pheromones and bamboo volatiles. *Proc. Natl. Acad. Sci. U.S.A.* **2017**, *114* (46), No. E9802-E9810.